Radium single-ion optical clock

Versolato, O. O.; Wansbeek, L. W.; Jungmann, K.; Timmermans, R. G. E.; Willmann, L.; Wilschut, H. W.

Radium single-ion optical clock

O. O. Versolato,[1] L. W. Wansbeek,[1] K. Jungmann,[1]

R. G. E. Timmermans,[1] L. Willmann,[1] and H. W. Wilschut[1]

[1]*KVI, University of Groningen, Zernikelaan 25,*

9747 AA Groningen, The Netherlands

(Dated: February 25, 2011)

Abstract

We explore the potential of the electric quadrupole transitions $7s\,^2S_{1/2}$ - $6d\,^2D_{3/2}$, $6d\,^2D_{5/2}$ in radium isotopes as single-ion optical frequency standards. The frequency shifts of the clock transitions due to external fields and the corresponding uncertainties are calculated. Several competitive ^{A}Ra$^+$ candidates with $A = 223$ - 229 are identified. In particular, we show that the transition $7s\,^2S_{1/2}\,(F = 2, m_F = 0)$ - $6d\,^2D_{3/2}\,(F = 0, m_F = 0)$ at 828 nm in ^{223}Ra$^+$, with no linear Zeeman and electric quadrupole shifts, stands out as a relatively simple case, which could be exploited as a compact, robust, and low-cost atomic clock operating at a fractional frequency uncertainty of 10^{-17}. With more experimental effort, the ^{223,225,226}Ra$^+$ clocks could be pushed to a projected performance reaching the 10^{-18} level.

I. INTRODUCTION

Optical atomic clocks based on ultranarrow optical transitions in single laser-cooled trapped ions have demonstrated a stability and accuracy significantly better than the [133]Cs atom microwave frequency standard. Transitions in various ions are presently under investigation as candidates for optical frequency standards, including electric quadrupole transitions in [40]Ca$^+$ [1, 2], [199]Hg$^+$ [3–5], [88]Sr$^+$ [6, 7], and [171]Yb$^+$ [8, 9], hyperfine-induced electric dipole transitions in [27]Al$^+$ [10–12], and [115]In$^+$ [13] and an electric octupole transition in [171]Yb$^+$ [14]; proposals also exist for [137]Ba$^+$ [15] and [43]Ca$^+$ [16]. These ion clocks currently operate at fractional frequency uncertainties $\delta\nu/\nu$ ranging from 10^{-16} to below 10^{-17}, with projected accuracies reaching the 10^{-18} level. The ultimate performance of each clock depends on the atomic structure of the ion, the sensitivity of the transition to the external environment, and the complexity of the experimental setup needed to operate the clock.

At our institute an experiment is in progress [17] to measure atomic parity violation in single Ra$^+$ ions [18]. This experimental setup can be adapted for an investigation of a single-ion Ra$^+$ clock. In this paper we explore the feasibility of using the strongly forbidden electric quadrupole transitions $7s\,^2S_{1/2}$ - $6d\,^2D_{3/2}$ at 828 nm and $7s\,^2S_{1/2}$ - $6d\,^2D_{5/2}$ at 728 nm in a single laser-cooled and trapped Ra$^+$ ion as a stable and accurate frequency standard [19–21]. Our studies are based on the available experimental information about the Ra$^+$ ion and on many-body atomic theory. The relevant energy levels of ^{223,225,226}Ra$^+$ and the proposed clock transitions are shown in Fig. 1. The $6d\,^2D_{3/2}$ and $6d\,^2D_{5/2}$ levels have a lifetime of 600 and 300 ms [20], respectively, corresponding to a Q factor $\sim 10^{15}$ for the clock transitions.

A major advantage of Ra$^+$ is that all the required wavelengths for cooling and repumping and for the clock transition can easily be made with off-the-shelf available semiconductor diode lasers, which makes the setup compact, robust, and low-cost compared to clocks that operate in the ultraviolet. Moreover, in odd radium isotopes clock transitions are available that are insensitive to electric quadrupole shifts of the metastable $6d\,^2D_J$ levels. Such shifts are an important limiting factor for several other ion clocks [22]. The radium isotopes under consideration are mostly readily available from low-activity sources.

Optical clocks are important tools to test the fundamental theories of physics. They are particularly useful in laboratory searches for possible spatial and temporal variations of
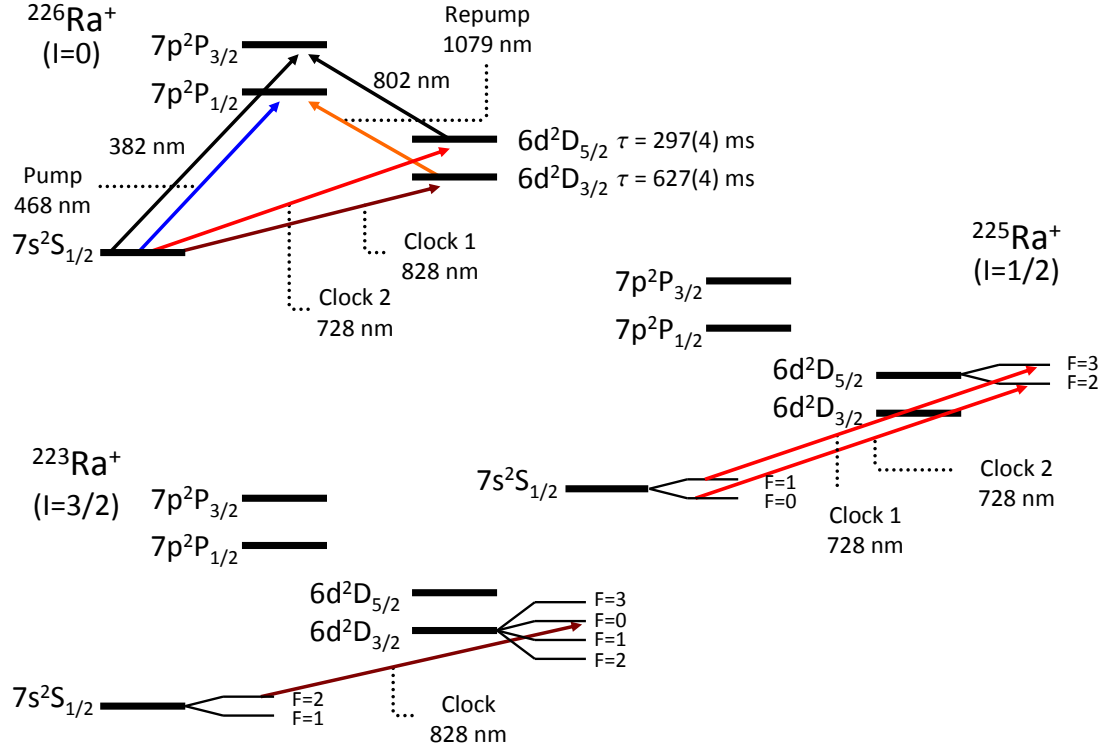
FIG. 1. (Color online) ^{223,225,226}Ra$^+$ level scheme with wavelengths taken from Ref. [23] and lifetimes from Ref. [20]. The clock transitions are indicated; in ^{225}Ra$^+$ and ^{226}Ra$^+$ two clock transitions are considered.

the physical constants that define these theories. Such searches are strongly motivated by cosmological theories that unify gravity and particle physics (see *e.g.* Ref. [24]). Laboratory tests have placed strong limits on the temporal variation of the electron-to-proton mass ratio m_e/m_p [25–27] and the fine-structure constant α. The most stringent limit on the latter was obtained by comparing two ultrasensitive ion clocks (^{27}Al$^+$ and ^{199}Hg$^+$) over the period of a year, yielding a limit $\dot{\alpha}/\alpha = (-1.6 \pm 2.3) \times 10^{-17}$/y [25]. The sensitivity to $\dot{\alpha}/\alpha$ results from relativistic contributions to the energy levels that are of order $\mathcal{O}(Z^2\alpha^2)$, favoring heavy atomic systems like ^{199}Hg$^+$. The Ra$^+$ clock transition has a comparably high intrinsic sensitivity [19, 20, 28] but of opposite sign to that of ^{199}Hg$^+$, making it a promising alternative candidate for testing the time variation of α. Ra$^+$ is also very sensitive to variations in the quark masses [29, 30].

TABLE I. Long-lived neutron-rich isotopes of radium with their lifetime and nuclear spin I [31], magnetic moments μ_I in units of μ_N [32] and quadrupole moments Q in barn [33]. Also shown are the decay series the isotopes occur in, and possible low-activity production sources; $A = 227$ and 229 have to be produced by nuclear reactions.

A	Half-life	I	μ_I	Q^{a}	Decay series	Source
223	11.43 d	3/2	0.2705(19)	1.254(66)	^{235}U	^{227}Ac (21.8 y)
224	3.66 d	0	0	0	^{232}Th	^{228}Th (1.9 y)
225	14.9 d	1/2	$-0.7338(5)$	0	^{233}U	^{229}Th (7.34 ky)
226	1.6 ky	0	0	0	^{238}U	^{226}Ra, ^{230}Th (75.4 ky)
227	42.2 m	3/2	$-0.4038(24)$	1.58(11)	-	-
228	5.75 y	0	0	0	^{232}Th	^{228}Ra
229	4.0 m	5/2	0.5025(27)	3.09(19)	-	-

$^{\mathrm{a}}$ The uncertainties were obtained by adding in quadrature the uncertainties given in Ref. [33].

II. RADIUM ISOTOPES

Radium offers a wide range of short- and long-lived isotopes with even and odd nuclear spin that could be considered for use as optical frequency standards. Only trace quantities of radium are needed to operate a single-ion Ra^+ clock, but demands on the half-life and the ease of production limit the options. The half-life of the isotope should be long compared to the excited $6d\,^2D_J$ level coherence time ($\sim$ seconds) required to address the ion with lasers. Further, it is preferable from an experimental point of view to be able to trap the ions for a longer time, at least a few minutes.

The light (neutron-poor) isotopes $A = 209$-214, with half-lives that range from several seconds up to a few minutes, have been produced at the KVI by fusion-evaporation reactions [17, 34]. A possible clock candidate could be $A = 213$, which has a half-life of 2.7 m; it is similar to the isotope $A = 225$, which we consider in detail below. We focus in this paper on the heavier (neutron-rich) isotopes with $A = 223$-229, because they have a half-life of longer than one minute, and, moreover, most of them occur in the decay series of uranium or thorium and therefore can be produced in sufficient quantities with a low-activity source, so that no accelerator is required. Table I gives an overview of these isotopes, with their

half-life, nuclear spin, and possible production methods. The nuclear magnetic moments and quadrupole moments listed are used to calculate the hyperfine constants of the $6d\,^2D_{3/2}$ and $6d\,^2D_{5/2}$ levels of the odd isotopes for which no experimental results are available.

For Ra$^+$ optical-clock purposes, the even isotopes $A = 224$, 226, and 228, with zero nuclear spin, are very similar and spectroscopically relatively simple. They are analogous to the ^{40}Ca$^+$ and ^{88}Sr$^+$ clocks. ^{226}Ra and ^{228}Ra are available as a source; ^{226}Ra$^+$ can also be taken from a ^{230}Th source, in which case there is no need to ionize the atoms. We limit ourselves to ^{226}Ra$^+$, which is the most easily available isotope, and we consider two transitions, namely $7s\,^2S_{1/2}$ - $6d\,^2D_{3/2}$ and $7s\,^2S_{1/2}$ - $6d\,^2D_{5/2}$, as indicated in Fig. 1.

In the odd isotopes, with nonzero nuclear spin, the presence of hyperfine structure gives two advantages. First, in all odd isotopes $m_F = 0 \leftrightarrow m'_F = 0$ transitions exist, which are insensitive to the linear Zeeman shift. Moreover, the odd isotopes offer several transitions between specific hyperfine levels that in first order do not suffer from the Stark shift due to the electric quadrupole moment of the $6d\,^2D_J$ level. In particular, we study the transition $7s\,^2S_{1/2}\,(F = 2, m_F = 0)$ - $6d\,^2D_{3/2}\,(F = 0, m_F = 0)$ in ^{223}Ra$^+$ (no linear Zeeman and quadrupole shifts) and $7s\,^2S_{1/2}\,(F = 1, m_F = 0)$ - $6d\,^2D_{5/2}\,(F = 3, m_F = \pm 2)$ in ^{225}Ra$^+$ (no quadrupole shift), see Fig. 1. In addition, we consider the transition $7s\,^2S_{1/2}\,(F = 0, m_F = 0)$ - $6d\,^2D_{5/2}\,(F = 2, m_F = 0)$ in ^{225}Ra$^+$ (no linear Zeeman shift), which resembles the ^{199}Hg$^+$ clock. We also include the isotopes $A = 227$ and 229, although their half-lives are rather short and they must be produced in nuclear reactions. Specifically, we consider the transitions $7s\,^2S_{1/2}\,(F = 2, m_F = 0)$ - $6d\,^2D_{3/2}\,(F = 0, m_F = 0)$ in ^{227}Ra$^+$ and $7s\,^2S_{1/2}\,(F = 2, m_F = 0)$ - $6d\,^2D_{5/2}\,(F = 0, m_F = 0)$ in ^{229}Ra$^+$; both transitions are free from linear Zeeman and quadrupole shifts.

III. SENSITIVITY TO EXTERNAL FIELD SHIFTS

All proposed optical frequency standards are sensitive to external perturbations due to the electric and magnetic fields present in the trap. These perturbations cause unwanted systematic shifts of the frequency of the clock transition. Although for a large part these shifts themselves can be corrected for, there is a remaining uncertainty associated with each shift due to limited experimental or theoretical accuracy. In this Section, we will investigate the sensitivity to the external fields of the candidate Ra$^+$ clock transitions for the different

isotopes. Input for the required atomic-structure quantities is taken from the recent KVI experiment [17] and from experiments at the ISOLDE facility at CERN [32, 33, 35]. The wavelengths of the relevant transition are taken from Ref. [23]. When no experimental data are available, we rely on atomic many-body theory calculations.

In the following, we briefly discuss the relevant shifts point-wise. The shift of the clock transition is defined as the shift of the excited $6d\,^2D_J$ level minus the shift of the $7s\,^2S_{1/2}$ ground state. The results of our calculations for the different Ra$^+$ isotopes are summarized below and divided into a *sensitivity*, see Table IV, and an *uncertainty*, see Table V. The theoretical expressions for the various external-field shifts can either be found in the literature or they are straightforward to derive; for completeness, the most important ones are given. In the following, we assume that one single laser-cooled radium ion is trapped in a radiofrequency (RF) electric quadrupole field, *i.e.* in a Paul trap.

A. Doppler shifts

The motion of an ion in a Paul trap can be described by a secular oscillation with a superimposed micromotion oscillation [36]. The micromotion oscillation is directly driven by the RF field applied to the trap. Any movement of the ion in the trap can, via the Doppler effect, cause broadening and shifts of the frequency of the clock transition. This effect is important even when the ion is laser-cooled to the Doppler limit. In the Lamb-Dicke regime [37], which can be reached by Doppler cooling on the strong $7s\,^2S_{1/2}$-$7p\,^2P_{1/2}$ transition at 468 nm, the oscillation amplitude is small compared to the laser-light wavelength, and first-order Doppler shifts are essentially negligible [38, 39]. Second-order Doppler shifts are still present. However, it can be shown that for a heavy ion like Ra$^+$ this shift is negligible in the Doppler cooling limit [16], with a projected fractional frequency uncertainty in the low 10^{-19} levels. It is, of course, a major challenge to achieve this limit experimentally [11]; excess micromotion of the ion, caused by electric fields that displace the ion from the middle of the RF pseudopotential, needs to be minimized.

6

TABLE II. The available experimental and theoretical hyperfine structure constants (in MHz) of the $7s\,^2S_{1/2}$, $6d\,^2D_{3/2}$, and $6d\,^2D_{5/2}$ levels of the relevant odd isotopes of Ra$^+$. The values A'_J for the isotopes for which no data was available were calculated with $A'_J = (I/I') \times (\mu'_I/\mu)A_J$, while for B_J we used $B'_J = (Q'/Q)B_J$. The reference values are printed bold. For the $7\,s^2S_{1/2}$ two different sets of experimental data were available; we used the underlined values. The experimental value for A_D of the $6d\,^2D_{3/2}$ level of ^{213}Ra was used to calculate A_D for the $6d\,^2D_{3/2}$ levels of the heavy isotopes; the ^{213}Ra magnetic moment used is $\mu_I = 0.6133(18)$ [32]. There are no data for the B_D coefficient of the $6d\,^2D_{3/2}$ level, nor for A_D and B_D of the $6d\,^2D_{5/2}$ level. Consequently, we used the theoretical values listed and estimated the uncertainty of the A_D coefficients of the $6d\,^2D_{5/2}$ to be 3%, and the uncertainty of all B_D coefficients conservatively as 10%.

			$7s\,^2S_{1/2}$	$6d\,^2D_{3/2}$		$6d\,^2D_{5/2}$	
			A_S	A_D	B_D	A_D	B_D
^{213}Ra$^+$	Expt.	[35]	22920.0(6.0)	-	0	-	0
	Expt.	[17]	-	**528(5)**	0	-	0
^{223}Ra$^+$	Expt.	[33]	3404.0(1.9)	-	-	-	-
	Expt.	[35]	3398.3(2.9)	-	-	-	-
	Theory	[20]	3567.26	77.08	**383.88**	-23.90	**477.09**
	Theory	[40]	3450	79.56	-	-24.08	-
^{225}Ra$^+$	Expt.	[33]	$-27731(13)$	-	0	-	0
	Expt.	[35]	$-27684(13)$	-	0	-	0
	Theory	[20]	-28977.76	-626.13	0	194.15	0
^{227}Ra$^+$	Expt.	[35]	$-5063.5(3.1)$	-	-	-	-
^{229}Ra$^+$	Expt.	[35]	3789.7(2.3)	-	-	-	-

B. Zeeman shifts

Magnetic fields in the trap lead to frequency shifts of the clock transition via the linear and quadratic Zeeman effect. For the transitions that suffer from the linear Zeeman effect it is hard to quantify the theoretical uncertainty, because the achievable accuracies depend on experimental details. In these cases, multiple transitions $m_F \leftrightarrow m'_F$ can be used to average out the linear effect to the desired level of accuracy. The linear Zeeman shift is absent in

7

$m_F = 0 \leftrightarrow m'_F = 0$ transitions, in which case the quadratic Zeeman shift $\Delta\nu_{\text{QZ}}$ becomes the dominant source of uncertainty. For the state $|\gamma, I, J; F, m_F\rangle$ it is given by

$$h\Delta\nu_{\text{QZ}}(\gamma, I, J, F, m_F) = (g_J\mu_B - g_I\mu_N)^2 B^2 J(J+1)(2J+1) \times$$

$$\sum_{F'} \left\{ \begin{matrix} J & F' & I \\ F & J & 1 \end{matrix} \right\}^2 \left(\begin{matrix} F & 1 & F' \\ -m_F & 0 & m_F \end{matrix} \right)^2 \frac{(2F+1)(2F'+1)}{E-E'} , \quad (1)$$

where the magnetic field B is taken along the z-axis; γ labels all quantum numbers that are not specified. We consider only couplings to the hyperfine-structure partners, since other contributions will be suppressed; therefore, the quadratic Zeeman effect is negligible in the even isotopes. The Zeeman shifts can be calculated from the hyperfine structure constants $A_{S,D}$ and B_D of the $7s\,^2S_{1/2}$, $6d\,^2D_{3/2}$, and $6d\,^2D_{5/2}$ levels, and the electron and nuclear g-factors. Table II lists the available experimental and theoretical values of $A_{S,D}$ and B_D of the relevant odd isotopes.

1. DC Zeeman shift

DC Zeeman shifts are caused by the static applied magnetic field present in the trap. We assume a magnetic field of 1 mG, which is a typical value needed to split the Zeeman degeneracies to order $\sim$10 kHz needed for proper state addressing. Passive shielding of an ion trap against magnetic fields has achieved $\leq 10\ \mu$G field stability [41]. This experimental number is taken as the uncertainty in the magnetic field strength in Table V. In order to calculate the uncertainty in the resulting shifts, the uncertainties in A_D and B_D, in the magnetic field ($\sim 10\ \mu$G), and in the g_J values were taken into account. For g_J the free-electron values were used with a conservative 1% uncertainty. The uncertainties due to g_I and the parameters associated with the $7s\,^2S_{1/2}$ state are negligible.

2. AC Zeeman shift

The RF voltages applied to the trap electrodes require rather large currents to flow. These currents give rise to an AC magnetic field in the trap center. In a perfect geometry, when the currents to all electrodes are equal, the individual contributions of the electrodes will cancel each other and the net magnetic field will be zero. However, this cancellation could be far from complete [25]. The oscillating magnetic field averages over the clock interrogation time

TABLE III. Dipole scalar, α_0^1, and tensor, α_2^1, polarizabilities, in units of $4\pi\varepsilon_0 a_0^3$, and quadrupole moments, Θ, in units of ea_0^2, for the $7s\,^2S_{1/2}$, $6d\,^2D_{3/2}$, and $6d\,^2D_{5/2}$ levels in Ra$^+$.

	Ref.	$7s\,^2S_{1/2}$	$6d\,^2D_{3/2}$	$6d\,^2D_{5/2}$
α_0^1	[21]	104.54(1.5)	83.71(77)	82.38(70)
	[40]	106.22		
α_2^1	[21]	-	$-50.23(43)$	$-52.60(45)$
Θ	[20]	-	2.90(2)	4.45(9)

(which is of the order of the $6d\,^2D_J$-level lifetime), which is long compared to typical RF periods (0.1-1 μs). Therefore, the expressions for the DC Zeeman effect can be used, with a rms magnetic field. For the ^{199}Hg$^+$ clock this magnetic field is conservatively estimated to be of the order $\sim$ mG [25]. We use 1 mG as estimate in Table V, because for Ra$^+$ the mass and other trapping parameters are similar. The resulting AC Zeeman shift proves to be one of the largest shifts. Therefore, it is important to work with a rather weak trap potential, as the average magnetic field scales with RF power. By varying the trap parameters the AC Zeeman shift can be measured. Moreover, averaging schemes that exploit the hyperfine structure could significantly reduce the uncertainty in the AC Zeeman shift. In this way it should be possible to reduce this uncertainty to the level of 25% of the shift itself; this is the uncertainty used in Tabel V.

C. Stark shifts

Stark shifts result both from static electric fields (causing DC Stark shifts) and from dynamic electric fields (causing AC Stark or light shifts). First, quadratic dipole Stark shifts are discussed, which are caused by the interaction of the dipole moment of the atom with the electric field. Next, we discuss quadrupole Stark shifts, caused by the interaction of the quadrupole moment of the atom with the gradient of the electric trap field; we look at both linear and quadratic quadrupole Stark shifts.

1. DC dipole Stark shift

The theory of the static quadratic dipole Stark shift was developed by Angel and Sandars [42]. For the state $|\gamma; J, m_J\rangle$ this shift is given by

$$h\Delta\nu_{\mathrm{DCDS}}(\gamma, J, m_J) = -\frac{1}{2}\alpha_0^1(\gamma, J)E^2 - \frac{1}{2}\alpha_2^1(\gamma, J)\frac{3m_J^2 - J(J+1)}{2J(2J-1)}(3E_z^2 - E^2) , \qquad (2)$$

where E is the DC electric field strength, α_0^1 and α_2^1 are the scalar and tensor polarizabilities, respectively. In Table III the available theoretical calculations for these polarizabilities are listed for the $7s\,^2S_{1/2}$, $6d\,^2D_{3/2}$, and $6d\,^2D_{5/2}$ levels in Ra$^+$; we used the results of Ref. [21] in our calculations. The polarizabilities for the hyperfine levels $|\gamma, I, J; F, m_F\rangle$ are calculated using

$$\alpha_k^1(\gamma, I, J, F) = (-1)^{J+I+F+k}(2F+1)\begin{Bmatrix} F & F & k \\ J & J & I \end{Bmatrix}\alpha_k^1(\gamma, J) . \qquad (3)$$

For an ion laser-cooled to the Lamb-Dicke regime, DC electric fields at the position of the ion can be reduced to < 10 V/m in the process of minimizing the micromotion [25]. This is the field uncertainty that we assume to estimate the fractional uncertainty in Table V in a worst case scenario, i.e. $E_z = E$.

The main source of DC dipole Stark shifts, however, is the presence of black-body (BB) radiation due to the nonzero temperature T of the trap and its surroundings. The energy shift of a level with dipole scalar polarizability α_0^1 in a BB electric field is given by [43]

$$h\Delta\nu_{\mathrm{BB}}(\gamma, J, m_J) = -\frac{1}{2}(8.319\,\mathrm{V/cm})^2\left(\frac{T(\mathrm{K})}{300}\right)^4\alpha_0^1(\gamma, J)(1+\eta) , \qquad (4)$$

where η is a small calculable term associated with dynamical corrections; it is of the order of a few percent [44] and therefore it can be neglected compared to the overall 10% uncertainty given in Table IV, which is mainly due to the theoretical uncertainties in the polarizabilities. The BB radiation is assumed to be isotropic, so the tensor polarizability plays no role. Since the BB radiation shift results in a relatively large fractional frequency uncertainty at room temperature $T = 293$ K (see Table V), the calculation was also performed for liquid-nitrogen temperature, $T = 77$ K (the ^{199}Hg$^+$ clock operates at 4 K). We assume an uncertainty in the temperature of 1 K, as in Ref. [45].

TABLE IV. Overview of the sensitivities to external-field shifts with the associated uncertainties between brackets: linear (LZ) and quadratic (QZ) Zeeman, dipole Stark (DS) DC and AC, and linear or quadratic quadrupole Stark (QS). The quoted uncertainties are derived from a Monte Carlo model, taking into account the uncertainties for all parameters as quoted in the text and previous Tables; $t \equiv (3E_z^2 - E^2)/(2E^2)$ parametrizes the tensor part of the DC dipole Stark shift.

Isotope	Transition	LZ	QZ	DS DC	DS AC	QS
			mHz/mG²	mHz V⁻² cm²	mHz μW mm⁻²	mHz V⁻¹ cm²
^{223}Ra$^+$	$7s\,^2S^{F=2,m_F=0}_{1/2}$ - $6d\,^2D^{F=0,m_F=0}_{3/2}$	no	4.9(7)	2.6(2)	0.72(4)	$15(2) \times 10^{-9}$ [a]
^{225}Ra$^+$(1)	$7s\,^2S^{F=1,m_F=0}_{1/2}$ - $6d\,^2D^{F=3,m_F=\pm2}_{5/2}$	yes	0.75(3)	2.8(2)	1.6(3)	$6.2(3) \times 10^{-9}$ [a]
^{225}Ra$^+$(2)	$7s\,^2S^{F=0,m_F=0}_{1/2}$ - $6d\,^2D^{F=2,m_F=0}_{5/2}$	no	$-1.28(5)$	$2.8(2) - 5.23(5)t$	1.2(3)	24.1(5)
^{226}Ra$^+$(1)	$7s\,^2S^{m_J=\pm\frac{1}{2}}_{1/2}$ - $6d\,^2D^{m_J=\pm\frac{3}{2}}_{3/2}$	yes	0	$2.6(2) + 6.25(5)t$	0.9(2)	$-19.6(1)$
^{226}Ra$^+$(2)	$7s\,^2S^{m_J=\pm\frac{1}{2}}_{1/2}$ - $6d\,^2D^{m_J=\pm\frac{3}{2}}_{5/2}$	yes	0	$2.8(2) - 1.30(1)t$	1.5(4)	6.0(1)
^{227}Ra$^+$	$7s\,^2S^{F=2,m_F=0}_{1/2}$ - $6d\,^2D^{F=0,m_F=0}_{3/2}$	no	2.8(2)	2.6(2)	0.72(4)	$5.9(4) \times 10^{-9}$ [a]
^{229}Ra$^+$	$7s\,^2S^{F=2,m_F=0}_{1/2}$ - $6d\,^2D^{F=0,m_F=0}_{5/2}$	no	27(3)	2.8(2)	1.6(3)	$12(1) \times 10^{-9}$ [a]
^{43}Ca$^+$	$4s\,^2S^{F=4,m_F=0}_{1/2}$ - $3d\,^2D^{F=6,m_F=0}_{5/2}$	no	90.5 [16]	$5.6(4) + 2.1(2)t$ [16]	8(8) [16]	8.1 [16]
^{199}Hg$^+$	$5d^{10}6s\,^2S^{F=0,m_F=0}_{1/2}$ - $5d^96s^2\,^2D^{F=2,m_F=0}_{5/2}$	no	0.18925(28) [46]	-1.14 [46]	$-$[b]	-3.6 [46]
^{88}Sr$^+$	$5s\,^2S^{m_J=\pm1/2}_{1/2}$ - $4d\,^2D^{m_J=\pm5/2}_{5/2}$	yes	0	4.6(2) [22]	-2.24 [47]	$-18(2)$ [48]

[a] These are second-order quadrupole shifts with units mHz (V⁻¹ cm²)².

[b] The uncertainty caused by the AC Stark shift was measured to contribute less than 2×10^{-17} to the fractional frequency uncertainty [4].

TABLE V. Overview of the shifts, in mHz, due to the external fields with the associated uncertainties between brackets. The values and uncertainties are derived from those in Table IV, taking into account the field uncertainties as explained in the text. At the bottom of the Table the resulting fractional frequency uncertainties $\delta\nu/\nu$ caused by the external-field shifts are given for different scenarios; $\delta\nu$ indicates the uncertainty in a certain shift, rather than the shift itself. The transitions for the different isotopes are as given in Table IV.

Shift	^{223}Ra$^+$	^{225}Ra$^+$(1)	^{225}Ra$^+$(2)	^{226}Ra$^+$(1)	^{226}Ra$^+$(2)	^{227}Ra$^+$	^{229}Ra$^+$
LZ	no	yes	no	yes	yes	no	no
QZ, DC	4.9(7)	0.74(3)	$-1.28(5)$	0	0	2.8(2)	27(3)
QZ, AC	(1.2)	(0.19)	(-0.32)	0	0	(0.7)	(6.8)
BB, 293(1) K	163(14)	173(13)	173(13)	163(13)	174(13)	163(13)	174(13)
BB, 77(1) K	0.78(8)	0.83(8)	0.83(8)	0.78(8)	0.83(7)	0.78(7)	0.83(8)
DS, DC Scalar	(0.026)	(0.028)	(0.028)	(0.026)	(0.028)	(0.026)	(0.028)
DS, DC Tensor	0	0	(-0.05)	(-0.06)	(-0.013)	0	0
DS, AC	0.72(4)	1.6(3)	1.2(3)	0.9(2)	1.5(4)	0.72(4)	1.6(3)
QS	1.5(2)	0.62(3)	$(24.1)\times10^3$	$(-19.6)\times10^3$	$(6.0)\times10^3$	0.59(4)	1.2(1)
Total shift (293 K)	170(14)	177(13)	$(24)\times10^3$	$(20)\times10^3$	$(6.0)\times10^3$	167(14)	203(15)
Total shift (77 K)	7.9(1.4)	3.8(4)	$(24)\times10^3$	$(20)\times10^3$	$(6.0)\times10^3$	4.9(7)	30(7)
Total shift (293 K, no QS)			173(13)	164(13)	175(13)		
Total shift (77 K, no QS)			0.7(4)	1.5(2)	2.3(4)		
Total $\delta\nu/\nu$ (293 K)	3.7×10^{-17}	3.2×10^{-17}	5.9×10^{-14}	5.4×10^{-14}	1.5×10^{-14}	3.7×10^{-17}	3.6×10^{-17}
Total $\delta\nu/\nu$ (77 K)	4.0×10^{-18}	9.1×10^{-19}	5.9×10^{-14}	5.4×10^{-14}	1.5×10^{-14}	2.1×10^{-18}	1.7×10^{-17}
Total $\delta\nu/\nu$ (293 K, no QS)			3.2×10^{-17}	3.7×10^{-17}	3.3×10^{-17}		
Total $\delta\nu/\nu$ (77 K, no QS)			1.1×10^{-18}	4.9×10^{-19}	9.1×10^{-19}		

2. AC dipole Stark shift

The most important cause of AC dipole Stark shifts is the laser locked to either the 728 nm or 828 nm clock transition, since we assume that the cooling and probing lasers are fully extinguished at the time of measurement. When the laser propagates along the z-axis, the AC dipole Stark shift of a state $|\gamma, J, m_J\rangle$ is given by [49]

$$h\Delta\nu_{\mathrm{ACDS}}(\gamma, J, m_J; \nu_L) = -\frac{I_L}{2\varepsilon_0 c}\left(\alpha_0^1(\nu_L) + A\,\alpha_1^1(\nu_L)\frac{m_J}{2J} - \alpha_2^1(\nu_L)\frac{3m_J^2 - J(J+1)}{2J(2J-1)}\right) , \quad (5)$$

where I_L is the intensity of the laser which we take as 1 μW/mm^2, ν_L is its frequency at the clock transition, and A is a numerical factor whose value depends on the type of polarization. Further, $\alpha_0^1(\nu_L)$, $\alpha_1^1(\nu_L)$, and $\alpha_2^1(\nu_L)$ are the dynamic scalar, vector, and tensor polarizability, respectively, of the state $|\gamma, J, m_J\rangle$. We choose the polarization such that $A = 0$, therefore we only need the scalar and tensor polarizabilities. These are given by

$$\alpha_0^1(\gamma, J; \nu_L) = -\frac{2}{3(2J+1)}\sum_{\gamma' J'}|\langle\gamma' J'||D||\gamma J\rangle|^2\frac{\Delta E}{(\Delta E)^2 - (h\nu_L)^2} , \quad (6)$$

$$\alpha_2^1(\gamma, J; \nu_L) = -4\sqrt{\frac{5}{6}}\left(\frac{J(2J-1)}{(2J+3)(J+1)(2J+1)}\right)^{1/2}(-1)^{2J} \times$$

$$\sum_{\gamma' J'}(-1)^{J-J'}\begin{Bmatrix}1 & 1 & 2\\ J & J & J'\end{Bmatrix}|\langle\gamma' J'||D||\gamma J\rangle|^2\frac{\Delta E}{(\Delta E)^2 - (h\nu_L)^2} , \quad (7)$$

with $\Delta E = E - E'$ and D the dipole operator. For $\nu_L \to 0$, the above equations reduce to their static counterparts. In calculating the dynamic polarizabilities we use the values for the dipole matrix elements given in Refs. [40, 50, 51]. In using this sum over the valence states approach, we do not take the core contributions, which are of order 10% [20], into account. However, the core contributions cancel since we look at differential shifts, and these contributions are common. The remaining uncertainty is due to neglected higher-order valence and valence-core couplings, and the uncertainty in the dipole matrix elements.

3. Quadrupole Stark shift

The interaction of the atomic quadrupole moment with the gradient of an electric field gives rise to an electric quadrupole shift. This shift is troublesome in several optical frequency

standards [22]. The expression used for the linear quadrupole Stark shift is [46]

$$h\Delta\nu_{\mathrm{LQS}}(\gamma, I, J, F, m_F) = A_{\mathrm{DC}}\Theta(\gamma, J)\frac{2\left[F(F+1) - 3m_F^2\right](2F+1)}{[(2F+3)(2F+2)(2F+1)2F(2F-1)]^{1/2}}$$

$$\times (-1)^{I+J+F} \begin{Bmatrix} J & 2 & J \\ F & I & F \end{Bmatrix} \begin{pmatrix} J & 2 & J \\ -J & 0 & J \end{pmatrix}^{-1} X , \qquad (8)$$

where A_{DC} is the electric field gradient, $\Theta(\gamma, J)$ the quadrupole moment, and X contains the angular factors resulting from the rotation of the quadrupole field frame to the quantization axis [46]. The quadrupole moment of the $7s\,^2S_{1/2}$ ground state is zero, those of the $6d\,^2D_{3/2}$ and $6d\,^2D_{5/2}$ levels [20] are listed in Table III. There are three special cases in which the first-order effect also vanishes for particular hyperfine states of the $6d\,^2D_J$ levels:

(i) $F = 0$ levels have no quadrupole moment; this applies to the ^{223,227,229}Ra$^+$ cases.

(ii) When $F = 2$, $I = 3/2$, $J = 3/2$, the $6j$-symbol in Eq. (8) is zero. This set of quantum numbers is available in ^{223,227}Ra$^+$, however, there is no improvement over the previous case (i). All other shifts and associated uncertainties were calculated to be equal to, or larger than, their counterparts in the $F = 0$ case. Therefore, these transitions have not been included in Tables IV and V.

(iii) For $F = 3$, $m_F = \pm 2$ the shift vanishes because of the factor $F(F+1) - 3m_F^2$ in Eq. (8); this applies to the ^{225}Ra$^+$(1) case.

The transitions in ^{226}Ra$^+$ and ^{225}Ra$^+$(2) do suffer from a linear quadrupole shift. These are given in Tables IV and V. To estimate the size of these shifts and their uncertainties, we assumed that in the trap a typical static stray electric field gradient $A_{\mathrm{DC}} \simeq 10^3$ V/cm^2 is present due to patch potentials. We assume that the angular factor X is of order 1. Since the orientation of the stray field is unknown, we take the full shift as an estimate of the uncertainty. The effects of the much larger RF trapping fields average out over the interrogation period.

However, the transitions that are free from the linear effect do suffer from a second-order, quadratic quadrupole Stark shift. This contribution is significant because now the effects from the RF trap potential do not average out. This RF potential gives rise to a typical rms field gradient $A_{\mathrm{AC}} = 10^4$ V/cm^2. To estimate the size of the shift we assume that the

magnetic-field orientation and the z-axis of the quadrupole trap field coincide. Taking only couplings to hyperfine partners into account results in

$$h\Delta\nu_{\mathrm{QQS}}\left(\gamma, I, J, F, m_F\right) = 4A_{\mathrm{AC}}^2\Theta(\gamma, J)^2 \sum_{F'} \frac{(2F+1)(2F'+1)}{E-E'}$$

$$\times \begin{pmatrix} F' & 2 & F \\ -m_F & 0 & m_F \end{pmatrix}^2 \begin{Bmatrix} J & F' & I \\ F & J & 2 \end{Bmatrix}^2 \begin{pmatrix} J & 2 & J \\ -J & 0 & J \end{pmatrix}^{-2}. \quad (9)$$

It should be feasible to achieve an overall 10% accuracy in the determination of this shift, which is the uncertainty quoted in Table V.

It can be seen in Table V that, similar to other clocks, the linear quadrupole shift is by far the largest shift in Ra$^+$. In ^{199}Hg$^+$ it was canceled by means of an averaging scheme [25, 46, 52], which brought down the uncertainty level to the 10^{-17} level. An alternative was presented more recently for ^{88}Sr$^+$ in Ref. [7], where it is projected that the uncertainty caused by the electric quadrupole shift can be reduced to the 10^{-18} level.

IV. DISCUSSION AND CONCLUSIONS

Tables IV and V contain the quantitative results of our studies. Table IV lists the sensitivities of the isotopes under study to the external fields. Also in Table IV the sensitivities of three other ion clocks that are based on an electric quadrupole transition are shown for comparison. In Table V, the Ra$^+$ sensitivities have been combined with typical values (and uncertainties) for the required and spurious external fields to quantify the resulting shifts and the fractional frequency uncertainties $\delta\nu/\nu$, where ν is the transition frequency and $\delta\nu$ the uncertainty in the total shift. In the top half of the Table the different shifts are given in mHz, with the corresponding uncertainty between brackets.

The transitions ^{225}Ra$^+$(1), ^{226}Ra$^+$(1), and ^{226}Ra$^+$(2) suffer from the linear Zeeman (LZ) shift, which therefore has to be controlled to the desired level of accuracy. The transitions ^{225}Ra$^+$(2), ^{226}Ra$^+$(1), and ^{226}Ra$^+$(2) suffer from a linear quadrupole Stark (QS) shift of the order 6-24 Hz, which has to be cancelled in order for these cases to be competitive. As mentioned, an averaging scheme was implemented for ^{199}Hg$^+$, a system comparable to ^{225}Ra$^+$(2), and 10^{-17} levels have been achieved [25, 52]. With an alternative averaging scheme, it appears feasible to reduce the QS shift experimentally to the 10^{-18} level in ^{88}Sr$^+$ [7], a system comparable to ^{226}Ra$^+$. The transitions in ^{223}Ra$^+$, ^{227}Ra$^+$, and ^{229}Ra$^+$ are

insensitive to both the LZ and the linear QS shifts, which is in principle a clear experimental advantage. The quadratic QS shifts are only of the order of 1 mHz. ^{227}Ra$^+$ is overall slightly better than ^{223}Ra$^+$, while ^{229}Ra$^+$ is worse, because it has a relatively large quadratic Zeeman (QZ) shift. As discussed, of these three, only ^{223}Ra can be obtained from a source.

Provided that the LZ and linear QS shifts can be cancelled in ^{225,226}Ra$^+$, the largest remaining shift is caused by the BB radiation. It is of order 0.2 Hz in all the isotopes. As in the case of ^{199}Hg$^+$, this shift can be rendered negligible by cooling down the system, albeit at the cost of a more complicated experimental setup. For that reason the BB shift is given for two temperatures, namely for room temperature (293 K) and for liquid-nitrogen temperature (77 K). The combination of these two options with the possibility of averaging away the QS shift (indicated by "no QS" in Table V) give us in total four different results for four sets of experimental choices, as shown in the bottom half of Table V. In the calculation of these uncertainties in the case "no QS," we have assumed that the LZ shift and the linear QS shift can be averaged out experimentally to negligible values. The actual obtainable accuracies in these cases depend on experimental details, but, as discussed, it appears realistic to aim for accuracy levels of a few times 10^{-18}.

We conclude that in particular the isotopes ^{223,225,226}Ra$^+$ are promising clock candidates with projected sensitivities that are all below the 10^{-17} level. The actual experimental feasibility of the scenarios discussed above remains to be demonstrated, of course. ^{223}Ra$^+$ stands out as an attractive simple candidate, without LZ and linear QS shifts, providing a compact, robust, and low-cost atomic clock.

V. SUMMARY

In summary, a theoretical analysis of the possible performance of a radium single-ion optical clock was presented. It was shown that transitions in several readily available Ra$^+$ isotopes are excellent candidates for alternative optical frequency standards. The advantages of a heavy single ion that can be directly laser-cooled and interrogated with off-the-shelf available semiconductor lasers are clear for many applications in which costs and system size and stability are of importance. Furthermore, Ra$^+$ is an excellent laboratory for the search for variation of fundamental constants, where it ranks among the most sensitive candidates.

VI. ACKNOWLEDGMENTS

[1] K. Matsubara, K. Hayasaka, Y. Ling, H. Ito, S. Nagano, M. Kajita, and M.Hosokawa, Appl. Phys. Express **1**, 067011 (2008).

[2] M. Chwalla, J. Benhelm, K. Kim, G. Kirchmair, T. Monz, M. Riebe, P. Schindler, A. S. Villar, W. Hänsel, C. F. Roos, R. Blatt, M. Abgrall, G. Santarelli, G. D. Rovera, and P. Laurent, Phys. Rev. Lett. **102**, 023002 (2009).

[3] S. A. Diddams, T. Udem, J. C. Bergquist, E. A. Curtis, R. E. Drullinger, L. Hollberg, W. M. Itano, W. D. Lee, C. W. Oates, K. R. Vogel, and D. J. Wineland, Science **293**, 825 (2001).

[4] W. H. Oskay, S. A. Diddams, E. A. Donley, T. M. Fortier, T. P. Heavner, L. Hollberg, W. M. Itano, S. R. Jefferts, M. J. Delany, K. Kim, F. Levi, T. E. Parker, and J. C. Bergquist, Phys. Rev. Lett. **97**, 020801 (2006).

[5] J. E. Stalnaker, S. A. Diddams, T. M. Fortier, K. Kim, L. Hollberg, J. C. Bergquist, W. M. Itano, M. J. Delany, L. Lorini, W. H. Oskay, T. P. Heavner, S. R. Jefferts, F. Levi, T. E. Parker, and J. Shirley, Appl. Phys. B **89**, 167 (2007).

[6] H. S. Margolis, G. P. Barwood, G. Huang, H. A. Klein, S. N. Lea, K. Szymaniec, and P. Gill, Science **306**, 1355 (2004).

[7] P. Dubé, A. A. Madej, J. E. Bernard, L. Marmet, J. S. Boulanger, and S. Cundy, Phys. Rev. Lett. **95**, 033001 (2005).

[8] T. Schneider, E. Peik, and C. Tamm, Phys. Rev. Lett. **94**, 230801 (2005).

[9] E. Peik, T. Schneider, and C. Tamm, J. Phys. B **39**, 145 (2006).

[10] T. Rosenband, P. O. Schmidt, D. B. Hume, W. M. Itano, T. M. Fortier, J. E. Stalnaker, K. Kim, S. A. Diddams, J. C. J. Koelemeij, J. C. Bergquist, and D. J. Wineland, Phys. Rev. Lett. **98**, 220801 (2007).

17

[11] C. W. Chou, D. B. Hume, J. C. J. Koelemeij, D. J. Wineland, and T. Rosenband, Phys. Rev. Lett. **104**, 070802 (2010).

[12] C. W. Chou, D. B. Hume, T. Rosenband, and D. J. Wineland, Science **329**, 1630 (2010).

[13] Y. H. Wang, R. Dumke, T. Liu, A. Stejskal, Y. N. Zhao, J. Zhang, Z. H. Lu, L. J. Wang, T. Becker, and H. Walther, Opt. Commun. **273**, 526 (2007).

[14] K. Hosaka, S. A. Webster, A. Stannard, B. R. Walton, H. S. Margolis, and P. Gill, Phys. Rev. A **79**, 033403 (2009).

[15] J. A. Sherman, W. Trimble, S. Metz, W. Nagourney, and N. Fortson, arXiv:0504013[physics.atom-ph] (2005).

[16] C. Champenois, M. Houssin, C. Lisowski, M. Knoop, G. Hagel, M. Vedel, and F. Vedel, Phys. Lett. A **331**, 298 (2004).

[17] O. O. Versolato, G. S. Giri, L. W. Wansbeek, J. E. van den Berg, D. J. van der Hoek, K. Jungmann, W. L. Kruithof, C. J. G. Onderwater, B. K. Sahoo, B. Santra, P. D. Shidling, R. G. E. Timmermans, L. Willmann, and H. W. Wilschut, Phys. Rev. A **82**, 010501(R) (2010).

[18] L. W. Wansbeek, B. K. Sahoo, R. G. E. Timmermans, K. Jungmann, B. P. Das, and D. Mukherjee, Phys. Rev. A **78**, 050501(R) (2008).

[19] V. A. Dzuba and V. V. Flambaum, Phys. Rev. A **61**, 034502 (2000).

[20] B. K. Sahoo, B. P. Das, R. K. Chaudhuri, D. Mukherjee, R. G. E. Timmermans, and K. Jungmann, Phys. Rev. A **76**, 040504(R) (2007).

[21] B. K. Sahoo, R. G. E. Timmermans, B. P. Das, and D. Mukherjee, Phys. Rev. A **80**, 062506 (2009).

[22] H. S. Margolis, J. Phys. B **42**, 154017 (2009).

[23] E. Rasmussen, Z. Phys. **86**, 24 (1933).

[24] J. D. Barrow, Ann. Phys. (Berlin) **19**, 202 (2010).

[25] T. Rosenband, D. B. Hume, P. O. Schmidt, C. W. Chou, A. Brusch, L. Lorini, W. H. Oskay, R. E. Drullinger, T. M. Fortier, J. E. Stalnaker, S. A. Diddams, W. C. Swann, N. R. Newbury, W. M. Itano, D. J. Wineland, and J. C. Bergquist, Science **319**, 1808 (2008).

[26] S. Blatt, A. D. Ludlow, G. K. Campbell, J. W. Thomsen, T. Zelevinsky, M. M. Boyd, J. Ye, X. Baillard, M. Fouché, R. L. Targat, A. Brusch, P. Lemonde, M. Takamoto, F.-L. Hong, H. Katori, and V. V. Flambaum, Phys. Rev. Lett. **100**, 140801 (2008).

[27] E. Reinhold, R. Buning, U. Hollenstein, A. Ivanchik, P. Petitjean, and W. Ubachs, Phys. Rev. Lett. **96**, 151101 (2006).

[28] V. V. Flambaum and V. A. Dzuba, `arXiv:0805.0462[physics.atom-ph]` (2008).

[29] V. V. Flambaum and A. F. Tedesco, Phys. Rev. C **73**, 055501 (2006).

[30] T. H. Dinh, A. Dunning, V. A. Dzuba, and V. V. Flambaum, Phys. Rev. A **79**, 054102 (2009).

[31] G. Audi, O. Bersillon, J. Blachot, and A. H. Wapstra, Nucl. Phys. **A729**, 3 (2003).

[32] E. Arnold, W. Borchers, M. Carre, H. T. Duong, P. Juncar, J. Lerme, S. Liberman, W. Neu, R. Neugart, E. W. Otten, M. Pellarin, J. Pinard, G. Ulm, J. L. Vialle, and K. Wendt, Phys. Rev. Lett. **59**, 771 (1987).

[33] W. Neu, R. Neugart, E. W. Otten, G. Passler, K. Wendt, B. Fricke, E. Arnold, H. J. Kluge, and G. Ulm, Z. Phys. D **11**, 105 (1989).

[34] P. D. Shidling, G. S. Giri, D. J. van der Hoek, K. Jungmann, W. Kruithof, C. J. G. Onderwater, M. Sohani, O. O. Versolato, L. Willmann, and H. W. Wilschut, Nucl. Instrum. Methods A **606**, 305 (2009).

[35] K. Wendt, S. A. Ahmad, W. Klempt, R. Neugart, E. W. Otten, and H. H. Stroke, Z. Phys. D **4**, 227 (1987).

[36] F. Mahor, V. Gheorghe, and G. Werth, *Charged Particle Traps* (Springer, 2005).

[37] D. Leibfried, R. Blatt, C. Monroe, and D. Wineland, Rev. Mod. Phys. **75**, 281 (2003).

[38] I. Lizuain, J. G. Muga, and J. Eschner, Phys. Rev. A **76**, 033808 (2007).

[39] D. Wineland and W. Itano, Phys. Rev. A **20**, 1521 (1979).

[40] R. Pal, D. Jiang, M. S. Safronova, and U. I. Safronova, Phys. Rev. A **79**, 062505 (2009).

[41] J. A. Sherman, T. W. Koerber, A. Markhotok, W. Nagourney, and E. N. Fortson, Phys. Rev. Lett. **94**, 243001 (2005).

[42] J. Angel and P. Sandars, Proc. Roy. Soc. A **305**, 125 (1968).

[43] B. Arora, M. S. Safronova, and C. W. Clark, Phys. Rev. **76**, 064501 (2007).

[44] S. G. Porsev and A. Derevianko, Phys. Rev. A **74**, 020502 (2006).

[45] T. Zelevinsky, G. K. Campbell, S. Blatt, M. M. Boyd, M. H. G. de Miranda, M. J. Martin, J. W. Thomsen, S. M. Foreman, J. Ye, T. M. Fortier, J. E. Stalnaker, S. A. Diddams, Y. L. Coq, Z. W. Barber, N. Poli, N. D. Lemke, K. M. Beck, and C. W. Oates, Science **319**, 1805 (2008).

[46] W. M. Itano, J. Research NIST **105**, 829 (2000).

[47] A. A. Madej, J. E. Bernard, P. Dubé, L. Marmet, and R. S. Windeler, Phys. Rev. A **70**, 012507 (2004).

[48] G. P. Barwood, H. S. Margolis, G. Huang, P. Gill, and H. A. Klein, Phys. Rev. Lett. **93**, 133001 (2004).

[49] P. Rosenbusch, S. Ghezali, V. A. Dzuba, V. V. Flambaum, K. Beloy, and A. Derevianko, Phys. Rev. A **79**, 013404 (2009).

[50] B. K. Sahoo, L. W. Wansbeek, K. Jungmann, and R. G. E. Timmermans, Phys. Rev. A **79**, 052512 (2009).

[51] U. I. Safronova, W. R. Johnson, and M. S. Safronova, Phys. Rev. A **76**, 042504 (2007).

[52] W. H. Oskay, W. M. Itano, and J. C. Bergquist, Phys. Rev. Lett. **94**, 163001 (2005).